

# Transient dynamics of the Anderson impurity model out of equilibrium

T. L. Schmidt,<sup>1</sup> P. Werner,<sup>2,3</sup> L. Mühlbacher,<sup>4</sup> and A. Komnik<sup>5</sup>

<sup>1</sup>*Departement Physik, Universität Basel, Klingelbergstr. 82, 4056 Basel, Switzerland*

<sup>2</sup>*Columbia University, 538 West 120th Street, New York, NY 10027, USA*

<sup>3</sup>*Theoretische Physik, ETH Zurich, 8093 Zurich, Switzerland*

<sup>4</sup>*Physikalisches Institut, Universität Freiburg, Hermann-Herder-Str. 3, 79104 Freiburg, Germany*

<sup>5</sup>*Institut für Theoretische Physik, Universität Heidelberg, Philosophenweg 19, 69120 Heidelberg, Germany*

(Dated: May 6, 2019)

We discuss the transient effects in the Anderson impurity model that occur when two fermionic continua with finite bandwidths are instantaneously coupled to a central level. We present results for the analytically solvable noninteracting resonant level system first and then consistently extend them to the interacting case using the conventional perturbation theory and recently developed nonequilibrium Monte Carlo simulation schemes. The main goal is to gain an understanding of the full time-dependent nonlinear current-voltage characteristics and the population probability of the central level. We find that, contrary to the steady state, the transient dynamics of the system depends sensitively on the bandwidth of the electrode material.

PACS numbers: 73.63.Kv, 73.63.-b, 5.10.Ln

## I. INTRODUCTION

The Anderson impurity model (AIM) has been introduced in the early 1960s to describe conduction electrons interacting with a magnetic atom and since then continues to attract the attention of condensed matter physicists.<sup>1</sup> Despite some notable exceptions,<sup>2</sup> for quite a long time mainly the zero-bias anomaly as well as other equilibrium properties, which can be extracted from the exact analytical solution via the Bethe ansatz approach, have been in the focus of the theoretical research.<sup>3,4,5,6</sup> It was only with the advent of nanotechnology that the investigation of nonequilibrium properties received a boost, as it became possible not only to directly manufacture structures which are adequately described by the AIM, but also to investigate their nonequilibrium properties under well controlled parameters.<sup>7,8,9</sup>

However, even in the time-independent steady-state case the analysis of the nonequilibrium situation turns out to be rather difficult. Despite a large number of works employing various perturbative and renormalization group techniques (e.g. Refs. [10,11,12,13,14,15,16,17]), or even attempts at solving the problem analytically,<sup>18</sup> there is no solution which unifies all known details.

Even more difficult is the case of the “preparative” nonequilibrium, i.e. the time evolution of the system from some initial preparation towards its steady state under a finite external voltage bias. For the first time this problem has been discussed in Ref. [19], where a solution for the wide flat band (WFB) limit was derived. However, the assumption of an infinitely wide band leads to the rather unphysical prediction of a displacement current which instantaneously jumps to a finite value immediately after switching on the tunneling.

The transient nonequilibrium dynamics of a strongly interacting quantum dot which is suddenly brought into the Kondo regime, has been investigated using approxi-

mative schemes.<sup>20,21</sup> Moreover, the band structure effects on the time evolution of noninteracting nanoscale devices have been investigated in [22].

However, the combined effect of interaction and finite bandwidth, both of which can be described within the framework of the AIM, have not yet been considered. In this article we attempt to address this issue by means of perturbation theory in the case of weak interactions and Monte Carlo (MC) simulations for moderate to strong interactions. Such results are not only interesting for future experiments. In view of recent attempts to use the integrability methods to understand the nonequilibrium properties of quantum impurity models it is important to develop and test numerical schemes which are able to generate reliable results for any parameter constellation.<sup>23,24,25</sup>

The structure of this paper is as follows. After introducing the system under consideration in Section II, we start with a resonant level model which maps onto the noninteracting AIM. Because the corresponding Hamilton operator is quadratic in the fermionic fields, the dynamics of the system can be investigated by analytic means at any parameter constellation even for a model with arbitrary band structure of the electrodes (cutoff schemes). The basis of our solution is the integral equation for the impurity retarded Green’s function (GF), which we derive next. It is then used in Section III for the calculation of the time-dependent impurity population function  $n(t)$  as well as for the expectation value of the transient current. Here we not only consider the simplest case of a WFB structure of the leads, but also more realistic models taking into account bandwidth effects. Section IV is devoted to the analysis of the transient dynamics of an interacting system. Using perturbation theory in interaction strength  $U$  we identify the leading order effects in that limit. A treatment of arbitrary interaction strengths is best accomplished with the help of a dedicated nonequilibrium Monte Carlo (MC) scheme,

which is presented in Section V.

## II. MODEL AND OBSERVABLES

The AIM Hamiltonian usually consists of four contributions,<sup>1</sup>

$$H = H_{\text{dot}} + H_0[\psi_{R,L}] + H_T + H_U. \quad (1)$$

$H_{\text{dot}}$  describes two spin-degenerate fermionic levels with energy  $\Delta$  (which we later shall also call ‘‘dot’’),

$$H_{\text{dot}} = \Delta \sum_{\sigma=\uparrow,\downarrow} d_{\sigma}^{\dagger} d_{\sigma}. \quad (2)$$

It is coupled to two fermionic continua – electrodes on the left and right sides. Each of these is modeled by a field operator  $\psi_{\alpha}(x)$  (where  $\alpha = L, R$ ) and the corresponding Hamiltonians  $H_0[\psi_{\alpha}]$ , whose precise shape we shall discuss in a moment. The operator  $H_T$  is responsible for the particle exchange between the dot and the electrodes and is given by a simple local tunneling term of the form

$$H_T = \sum_{\alpha=R,L} \sum_{\sigma} \gamma_{\alpha} [\psi_{\alpha\sigma}^{\dagger}(x=0) d_{\sigma} + \text{h.c.}] . \quad (3)$$

Finally,  $H_U$  accounts for the interaction in the system and is formally implemented as an additional energy cost for the double occupancy of the dot level,

$$H_U = U d_{\uparrow}^{\dagger} d_{\uparrow} d_{\downarrow}^{\dagger} d_{\downarrow}. \quad (4)$$

In general, it is quite difficult to analyze the properties of the interacting Anderson model at  $U \neq 0$ , but not impossible. In fact, at least in equilibrium an exact analytic solution can be derived via the Bethe ansatz.<sup>5,6</sup> In the genuine nonequilibrium, when a finite bias voltage is applied across the dot, the picture is far from complete since as yet no exact solution exists.

On the other hand, since the tunneling part  $H_T$ , being only quadratic in the fermionic operators, is diagonalizable by elementary methods and the Green’s functions (GFs) are accessible in all parameter regimes, the non-interacting system [aka resonant level (RL) model] is exactly solvable by elementary means.<sup>26</sup> In this case, the Hamiltonian as well as expectation values separate into spin-up and spin-down contributions, so that throughout this and the next Sections we shall work with spinless operators, recovering the necessary prefactors after the calculations.

In the case of the initially uncoupled dot GFs we have to deal with two different situations: (i) the dot level is empty,  $n_0 = 0$ , and (ii) the dot is populated by one electron,  $n_0 = 1$ . Due to the simple structure of  $H_{\text{dot}}$ , the time evolution is trivial,  $d(t) = d(0) \exp(-i\Delta t)$ , immediately leading to the following matrix (Keldysh) GF [27],

$$\mathbf{D}_0(t) = \begin{bmatrix} D_0(t) & D_0^<(t) \\ D_0^>(t) & \tilde{D}_0(t) \end{bmatrix} = e^{-i\Delta t} \begin{bmatrix} -i[\Theta(t)(1-n_0) - \Theta(-t)n_0] & in_0 \\ -i(1-n_0) & -i[\Theta(-t)(1-n_0) - \Theta(t)n_0] \end{bmatrix}, \quad (5)$$

where  $D_0(t)$  and  $\tilde{D}_0(t)$  denote the time-ordered and anti-time-ordered GFs, respectively. For the retarded and advanced components we obtain,

$$\begin{aligned} D_0^R(t) &= D_0(t) - D_0^<(t) = -i\Theta(t)e^{-i\Delta t}, \\ D_0^A(t) &= D_0^>(t) - \tilde{D}_0(t) = i\Theta(-t)e^{-i\Delta t}. \end{aligned} \quad (6)$$

The Hamiltonian for the electrode electrons can generally be written as (for  $\alpha = R, L$ )

$$H_0[\psi_{\alpha}] = \sum_{\mathbf{k}} \epsilon_{\mathbf{k}} \psi_{\alpha\mathbf{k}}^{\dagger} \psi_{\alpha\mathbf{k}}, \quad (7)$$

implying a trivial time evolution of the field operators. Due to the local tunneling assumption made in Eq. (3), coupling to the leads only involves the operator

$$\psi_{\alpha}(x=0) = \sum_{\mathbf{k}} \psi_{\alpha\mathbf{k}}. \quad (8)$$

Therefore, we only need *local* GFs of the band degrees of freedom in all subsequent calculations and can suppress the coordinate variable. For the retarded GF we thus have

$$g_{\alpha}^R(t) = -i\Theta(t) \int d\omega \rho(\omega) e^{-i\omega t}, \quad (9)$$

where we have introduced the energy-dependent density of states (DoS)  $\rho(\omega)$ . In a similar way, one obtains the full Keldysh matrix

$$\mathbf{g}_{\alpha}(\omega) = i2\pi\rho(\omega) \begin{bmatrix} f_{\alpha} - 1/2 & f_{\alpha} \\ -(1 - f_{\alpha}) & f_{\alpha} - 1/2 \end{bmatrix}. \quad (10)$$

Here,  $f_{\alpha}$  denotes the Fermi distribution function in the respective electrode  $\alpha = L, R$ .<sup>40</sup> The retarded and advanced components are easily retrieved,  $g_{\alpha}^R(\omega) = -i\pi\rho(\omega)$  and  $g_{\alpha}^A(\omega) = [g_{\alpha}^R(\omega)]^* = i\pi\rho(\omega)$ . We would

like to point out that the actual dimensionality of the electrode disappears from the problem during the transition from Eq. (7) to (9), since it is completely encoded in the DoS.

The GFs of the coupled system can be found analytically for arbitrary time dependence  $\gamma_\alpha(t) \neq 0$  of the tunneling constant. From now on, we shall concentrate on the case of sudden switching  $\gamma_\alpha(t) = \gamma_\alpha \Theta(t)$ , where  $\Theta(t)$  is the Heaviside step function. A generalization to arbitrary time dependence is relatively straightforward. The way to obtain the necessary Dyson equation is precisely the same as in the stationary case. The result can be summarized in the matrix equation<sup>19,26</sup> (for  $t, t' \geq 0$ ),

$$\mathbf{D}(t, t') = \mathbf{D}_0(t - t') + \int_0^\infty dt_1 \int_0^\infty dt_2 \times \mathbf{D}_0(t - t_1) \boldsymbol{\Sigma}(t_1 - t_2) \mathbf{D}(t_2, t'), \quad (11)$$

where the generalized self-energy is defined by

$$\boldsymbol{\Sigma}(t) = \gamma_L^2 \mathbf{g}_L(t) + \gamma_R^2 \mathbf{g}_R(t). \quad (12)$$

The seemingly complicated structure of Eq. (11) simplifies considerably for the retarded GF,

$$D^R(t, t') = D_0^R(t - t') + \int_0^\infty dt_2 K(t, t_2) D^R(t_2, t'), \quad (13)$$

where

$$K(t, t_2) = \int_0^\infty dt_1 D_0^R(t - t_1) \Sigma^R(t_1 - t_2) \quad (14)$$

is the kernel of the integral equation.

The simplest physical quantity to calculate is the time-dependent dot population  $n(t) = \langle d^\dagger(t) d(t) \rangle$ . It is convenient to rewrite it in terms of the off-diagonal Keldysh GF,

$$n(t) = -i D^<(t, t). \quad (15)$$

The necessary relation between this function and the already known retarded GF is provided by<sup>28,29</sup>

$$D^< = (1 + G^R \Sigma^R) D_0^< (1 + \Sigma^A G^A) + G^R \Sigma^< G^A, \quad (16)$$

where products denote integration over time. This relation is especially useful for the case of an initially empty dot since then  $D_0^< = 0$  and only the last term contributes. (A similar relation can be derived for the counterpart  $D_0^>$ , which would be useful for the initially populated dot.)

Another important observable is the current through the system. The canonical way to calculate it is to start from the total particle number operator,<sup>29</sup> e.g. in the left electrode  $Q_L$ , and to use the Heisenberg equation to obtain its time derivative, which is proportional to the current,

$$\begin{aligned} \hat{I}_L &= -\frac{dQ_L}{dt} = i[Q_L, H] \\ &= i\gamma_L (\psi_L^\dagger d - d^\dagger \psi_L). \end{aligned} \quad (17)$$

The evaluation of its expectation value then leads to mixed correlation functions of dot and lead operators,

$$I_L(t) = i\gamma_L \langle \psi_L^\dagger(t) d(t) \rangle - i\gamma_L \langle d^\dagger(t) \psi_L(t) \rangle. \quad (18)$$

The expectation values entering this formula can be rewritten in terms of GFs. After placing the time  $t$  on the forward Keldysh branch and performing the contour disentanglement we obtain (we use the definition  $D^K = D^< + D^>$ )

$$\begin{aligned} I_L(t) &= -\frac{\gamma_L^2}{2} \int_0^\infty dt_1 \{ [g_L^A(t, t_1) + g_L^K(t, t_1)] D^A(t_1, t) \\ &\quad + g_L^R(t, t_1) [D^K(t_1, t) + D^R(t_1, t)] \\ &\quad - [D^A(t, t_1) + D^K(t, t_1)] g_L^A(t_1, t) \\ &\quad - D^R(t, t_1) [g_L^K(t_1, t) + g_L^R(t_1, t)] \}. \end{aligned} \quad (19)$$

Some products of advanced and retarded GFs vanish as their factors have time arguments of opposite signs. This simplifies the result considerably,

$$I_L(t) = I'_L(t) + I''_L(t), \quad (20)$$

where

$$\begin{aligned} I'_L(t) &= \frac{\gamma_L^2}{2} \int_0^\infty dt_1 [D^K(t, t_1) g_L^A(t_1, t) \\ &\quad - g_L^R(t, t_1) D^K(t_1, t)] \\ &= -\gamma_L^2 \text{Re} \int_0^\infty dt_1 g_L^R(t, t_1) D^K(t_1, t), \end{aligned} \quad (21)$$

and

$$I''_L(t) = \gamma_L^2 \text{Re} \int_0^\infty dt_1 D^R(t, t_1) g_L^K(t_1, t), \quad (22)$$

after using the antihermiticity of the  $g^K$  and  $D^K$  GFs. For the evaluation of these expressions it is convenient to use the relation  $D^K = 2D^< + D^R - D^A$ .

### III. THE NONINTERACTING CASE

#### A. Wide flat band limit

In the stationary situation, the time-translational symmetry of all quantities entering Eqs. (13) and (14) is restored and the integral equation is solved by a mere Fourier transformation.<sup>26</sup> In the dynamic case, the situation is more complex. We begin with the already known results obtained in the approximation  $\rho(\omega) = \rho_0$ , when the conduction band in the electrodes is assumed to be of zero curvature over an infinite range of energies. In this case (we concentrate henceforth on the symmetric coupling case  $\gamma = \gamma_R = \gamma_L$ )

$$\begin{aligned} g_\alpha^A(t) &= i\pi\rho_0 \delta(t), \\ g_\alpha^R(t) &= -i\pi\rho_0 \delta(t), \end{aligned} \quad (23)$$

$$K(t, t_2) = -\Gamma e^{-i\Delta(t-t_2)} \Theta(t-t_2) \Theta(t_2), \quad (24)$$

where  $\Gamma = 2\pi\rho_0\gamma^2$ . As has been realized in Refs. [30,19], the integral equation for the retarded GF can then be solved by iterations. The result has the very appealing form

$$D^R(t-t') = -i\Theta(t-t') e^{-i\Delta(t-t')} e^{-\Gamma(t-t')}. \quad (25)$$

Gathering all terms we obtain

$$\begin{aligned} n(t) &= \frac{\Gamma}{2\pi} \int d\omega [f_R(\omega) + f_L(\omega)] \cdot \\ &\times \frac{1 + e^{-2\Gamma t} - 2e^{-\Gamma t} \cos[(\omega - \Delta)t]}{\Gamma^2 + (\omega - \Delta)^2}, \\ &= n_{\text{stat}}(1 + e^{-2\Gamma t}) \\ &- \frac{\Gamma e^{-\Gamma t}}{\pi} \int d\omega [f_R(\omega) + f_L(\omega)] \frac{\cos[(\omega - \Delta)t]}{\Gamma^2 + (\omega - \Delta)^2}. \end{aligned} \quad (26)$$

The asymptotic, steady-state value for the population is given by

$$\begin{aligned} n_{\text{stat}} &= \frac{\Gamma}{2\pi} \int d\omega \frac{f_R(\omega) + f_L(\omega)}{\Gamma^2 + (\omega - \Delta)^2} \\ &= \frac{1}{2} + \frac{1}{2\pi} \text{Im} \sum_{p=\pm} \Psi \left( \frac{1}{2} + \frac{\Gamma}{2\pi T} + i \frac{pV/2 - \Delta}{2\pi T} \right), \end{aligned} \quad (27)$$

where  $\Psi(x)$  denotes the psi (digamma) function. In the simpler case of zero temperature, it simplifies to

$$n_{\text{stat}} = \frac{1}{2} + \frac{1}{2\pi} \sum_{p=\pm} \arctan(pV/2 - \Delta). \quad (28)$$

Already in Eq. (26) one easily identifies the tunneling rate  $\Gamma$  as the energy scale which governs the approach to the steady state. Indeed, at almost all values of other parameters the steady state (in which we can still have a finite transport current) is established after a time of the order  $\Gamma^{-1}$ . The current which is flowing during this time onto and from the dot (depending on the initial condition) is to a large extent the displacement current<sup>31,32</sup> which is given by the time derivative of  $n(t)$ ,

$$\begin{aligned} I_{\text{disp}}(t) &= -\frac{dn(t)}{dt} \\ &= \frac{\Gamma e^{-\Gamma t}}{\pi} \int d\omega [f_L(\omega) + f_R(\omega)] \\ &\times \frac{\Gamma e^{-\Gamma t} - \Gamma \cos[(\omega - \Delta)t] - (\omega - \Delta) \sin[(\omega - \Delta)t]}{\Gamma^2 + (\omega - \Delta)^2}. \end{aligned} \quad (29)$$

A surprising effect is found if the dot energy is higher than the Fermi edges in the electrodes: on the intermediate time scale  $\Delta^{-1}$ , the dot population shoots over its asymptotic steady-state value and reaches a local maximum despite the absence of any kind of interactions. The subsequent relaxation to  $n_{\text{stat}}$  may then be either smooth, or accompanied by a number of oscillations, as shown in Fig. 1. These are remnants of the oscillatory behavior of the integrand in Eq. (26) and have a period  $\sim \Delta^{-1}$ . In

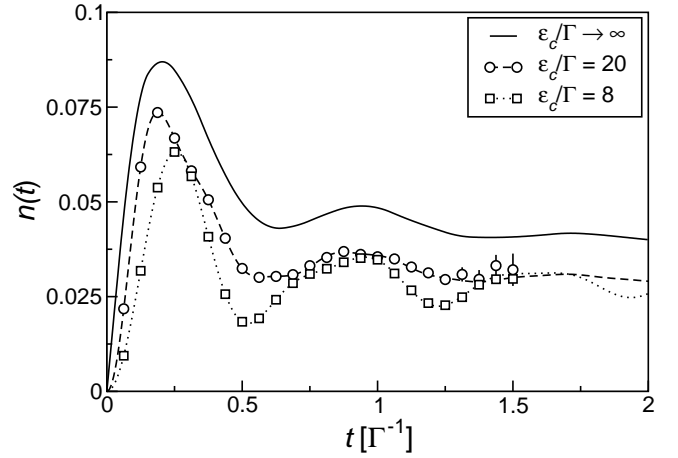


FIG. 1: Population of the noninteracting dot as a function of time measured in units of  $\Gamma^{-1}$  for  $V = 0$ ,  $\Delta/\Gamma = 8$  and different bandwidths: for  $\epsilon_c/\Gamma = 8, 20, \infty$ . Curves are the analytic results, symbols represent the MC simulation data (see Section V).

the opposite limit of a dot lying far below the chemical potentials in the leads, one does not observe related effects. However, as the system is particle-hole symmetric, the analogous population oscillations are recovered for the initially populated dot.

Next we investigate the time-dependent current. The first contribution is essentially given by the time-dependent  $n(t)$ ,

$$I'_L(t) = \frac{\Gamma}{2} \Theta(t) [1 - 2n(t)], \quad (30)$$

leading to

$$\begin{aligned} I_L(t) &= I_{L,\text{stat}} - \Gamma e^{-\Gamma t} \int \frac{d\omega}{2\pi} \frac{1}{(\omega - \Delta)^2 + \Gamma^2} \\ &\times \{ \Gamma e^{-\Gamma t} [f_R(\omega) + f_L(\omega)] - \Gamma \cos[(\omega - \Delta)t] [2f_R(\omega) + 1] \\ &- (\omega - \Delta) \sin[(\omega - \Delta)t] [2f_L(\omega) - 1] \}, \end{aligned} \quad (31)$$

where the asymptotic steady-state value of the current is

$$\begin{aligned} I_{L,\text{stat}} &= \Gamma^2 \int \frac{d\omega}{2\pi} \frac{f_L(\omega) - f_R(\omega)}{(\omega - \Delta)^2 + \Gamma^2} \\ &= \Gamma G_0 \text{Im} \sum_{p=\pm} p \Psi \left( \frac{1}{2} + \frac{\Gamma}{2\pi T} + i \frac{pV/2 - \Delta}{2\pi T} \right), \end{aligned} \quad (32)$$

with  $G_0 = e^2/h$  being the conductance quantum. The current  $I_R(t)$  through the right contact is by symmetry found from  $I_R(V, t) = -I_L(-V, t)$ . The difference in currents through the individual contacts describes the charge redistribution in the system, i.e. it must be equal to the displacement current (29),

$$I_{\text{disp}}(t) = I_L(V, t) + I_L(-V, t), \quad (33)$$

which is shown by inspection. The total current through

the AIM then becomes<sup>33</sup>

$$\begin{aligned} I(V, t) &= [I_L(V, t) + I_R(V, t)] / 2 \\ &= [I_L(V, t) - I_L(-V, t)] / 2. \end{aligned} \quad (34)$$

The last two identities imply a very convenient representation of the currents through the contacts

$$I_{L,R}(t) = I(t) \pm I_{\text{disp}}(t) / 2. \quad (35)$$

Note the instantaneous current value at  $t = 0$ ,

$$I_L(0) = \Gamma^2 \int \frac{d\omega}{2\pi} \frac{1}{(\omega - \Delta)^2 + \Gamma^2} = \frac{\Gamma}{2}, \quad (36)$$

which is independent of both voltage *and*  $\Delta$ . In fact,  $I_L(0)$  corresponds to the current through the resonant level system in the case of *infinitely* high applied voltage. This unphysical, *instantaneous* current onset of the left current comes as no surprise since initially every electron in the band has the same probability of populating the empty dot, while electrons with arbitrarily high energies allow correspondingly fast processes. Obviously, such a situation can never occur in any real system due to a strictly finite width of the electrodes' conductance bands. To comply with this restraint, we proceed with analyzing a more realistic model with finite bandwidths.

## B. AIM with soft cutoff

Depending on the material, the method of coupling to the voltage sources, and measurement apparatus the electrode band structure can be more complicated than for the WFB. The simplest model is a rigid flat band with a constant DoS  $\rho_0$  between  $\epsilon'_c$  and  $\epsilon_c$ , which represent the band bottom and upper boundary, respectively, and zero otherwise. A more sophisticated scheme, which is more physical involves soft cutoffs at  $\epsilon_c$  and  $\epsilon'_c$ . Mathematically, they can be realized as

$$\rho(\omega) = \frac{\rho_0}{e^{(\omega - \epsilon_c)/\eta} + 1} \left( 1 - \frac{1}{e^{(\omega - \epsilon'_c)/\eta} + 1} \right), \quad (37)$$

where  $\eta$  is a softening parameter. From the physical point of view one obvious 'good' value for it would be  $\eta = T$ , which is the value we are using for numerical plots.<sup>41</sup> The choice of two different values,  $\epsilon_c$  and  $\epsilon'_c$ , is deliberate. While in the equilibrium, when no bias voltage is applied to the system,  $\epsilon'_c = -\epsilon_c$  covers the relevant physics whatever the band filling (as long as the chemical potentials are not too close to the band boundaries), the situation is more delicate when out of equilibrium. Usually, the finite voltage is realized by different chemical potentials  $\mu_{L,R}$  of the two electrodes. Changing them around the equilibrium value (we always assume the band to be half-filled, so that in equilibrium  $\mu_{L,R} = 0$  in our choice of zero point of energy) without shifting the band boundaries would imply charging of the electrodes. In

order to avoid this, one has to shift the complete band along with the changed chemical potential to ensure the electroneutrality,  $\epsilon_c \rightarrow \epsilon_c + \mu_{L,R}$ , and  $\epsilon'_c \rightarrow -\epsilon_c + \mu_{L,R}$ . We shall see later that for voltages small compared to the band width  $2\epsilon_c$  the changes in observables vanish on a timescale of the order of  $\epsilon_c^{-1}$ . Nevertheless, in order to be consistent we shall keep two different values  $\epsilon_c$  and  $\epsilon'_c$ .

A stronger DoS energy dependence is expected for a system strongly coupled to its environment. In some cases even a DoS which vanishes at the Fermi level may emerge. Two notable situations are a system in the Coulomb blockade regime or a strongly interacting low-dimensional conductor in the Luttinger liquid phase. These are, however, systems with effectively interacting electrodes whose treatment we postpone to a follow-up publication. From now on, we would like to concentrate on the DoS (37).

In order to solve the Dyson equation (13) it is more convenient to have the retarded band GF in the time representation. According to the prescription (9) we find

$$g^R(t) = \pi \rho_0 \eta \Theta(t) \frac{e^{-i\epsilon'_c t} - e^{-i\epsilon_c t}}{[e^{(\epsilon'_c - \epsilon_c)/\eta} - 1] \sinh(\pi \eta t)}, \quad (38)$$

which is regular towards the limit  $t = 0$ . From this relation one can easily read off the retarded self-energy using Eq. (12). The corresponding integral equation kernel (14) turns out to depend only on the time difference ( $t - t_2$ ),

$$\begin{aligned} K(t - t_2) &= -i \frac{\Gamma T e^{-i\Delta(t-t_2)}}{1 - e^{(\epsilon_c - \epsilon'_c)/\eta}} \\ &\times \int_0^{t-t_2} d\tau e^{i\Delta\tau} \frac{e^{-i\epsilon'_c \tau} - e^{-i\epsilon_c \tau}}{\sinh(\pi \eta \tau)}. \end{aligned} \quad (39)$$

In fact, the last integral can be expressed in terms of hypergeometric functions. However, from a numerical point of view, it is more convenient to work with the integral (39) directly. In fact, writing down the equations for the retarded GFs in the steady state case and in the case of the sudden switching of tunneling one immediately realizes that they are identical in the relevant time domain. In order to calculate the time-dependent population function, one still can use the formula (16). The necessary off-diagonal self-energy is given by

$$\begin{aligned} \Sigma^<(t) &= -\frac{\Gamma T e^{-\epsilon_c/T}}{2 \sinh(\pi T t)} \sum_{i=R,L} \\ &\times \left[ \frac{e^{-i\mu_i t - \mu_i/T}}{(e^{-\mu_i/T} - e^{-\epsilon'_c/T})(e^{-\mu_i/T} - e^{-\epsilon_c/T})} \right. \\ &\quad \left. - \frac{e^{-i\epsilon'_c t - \epsilon'_c/T}}{(e^{-\epsilon'_c/T} - e^{-\epsilon_c/T})(e^{-\mu_i/T} - e^{-\epsilon'_c/T})} \right. \\ &\quad \left. + \frac{e^{-i\epsilon_c t - \epsilon_c/T}}{(e^{-\epsilon'_c/T} - e^{-\epsilon_c/T})(e^{-\mu_i/T} - e^{-\epsilon_c/T})} \right]. \end{aligned} \quad (40)$$

With the prerequisites (39) and (40) the calculation of the time evolution  $n(t)$  as well as of the currents is a

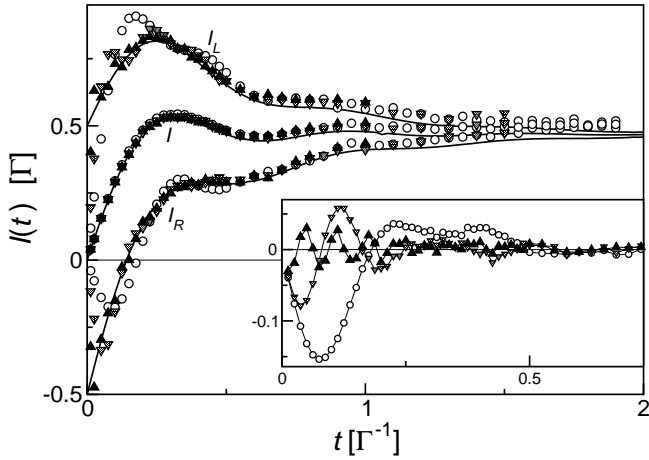


FIG. 2: DQMC data for the left, right, and total current  $I_{L,R}(t)$ , and  $I(t)$ , respectively, for  $U = \Delta = 0$ ,  $V = 20\Gamma$ , and  $T = 0.4\Gamma$ . Circles, triangles down, and triangles up refer to cutoff energies of  $\epsilon_c = 20\Gamma$ ,  $40\Gamma$ , and  $100\Gamma$ , respectively. The inset shows the difference in  $I(t)$  due to charge neutrality. The solid lines refer to the current calculated in the WFB limit via Eq. (31).

standard numerical task. The results of the calculations are presented in Figs. 1 and 2. The most drastic differences between the WFB model and that with a finite bandwidth are found in the short time behavior of the current. In contrast to the WFB prediction the instantaneous value of currents through individual contacts is strictly zero. Moreover, the slope (time derivative) of  $I_{L,R}(t)$  starts at zero rather than being finite. These differences eventually vanish after a timescale of the order  $\epsilon_c^{-1}$ , so that, as expected, the correspondence between the two calculation schemes improves. However, the actual current behavior becomes more oscillatory and prevents reliable simulations for too large  $\epsilon_c/\Gamma > 50$ . Contrary to the  $I_{L,R}(t)$  currents, the total current through the constriction is not only free of oscillations but also shows a far better agreement with the WFB model. We conclude that the finite bandwidth effects are contained almost completely in the displacement component of the current (29). Its behavior is plotted in Fig. 3.

Furthermore, we find a rather small difference between the results for systems which preserve and neglect the electroneutrality (see inset of Fig. 2), which only exists for times  $\sim \epsilon_c^{-1}$  and vanishes almost completely in the steady state. We would like to point out that the maximal deviation depicted in Fig. 2 is achieved for voltages half as large as the bandwidth. It is highly unlikely that such a situation can ever be realized in experiments, where the maximal voltages very seldom exceed 5% of  $2\epsilon_c$ . Therefore from now on we refrain from implementing the electroneutrality requirement in our analysis.

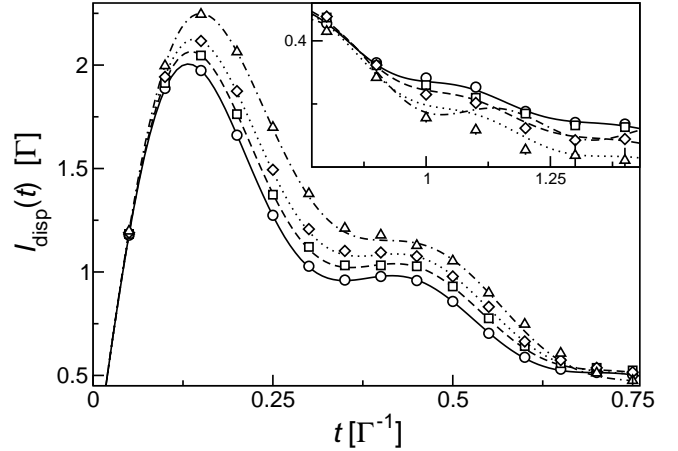


FIG. 3: DQMC data for the displacement current  $I_{\text{disp}}(t)$  (open symbols) and results according to the perturbation theory (lines) for  $V = 0$ ,  $\epsilon_c = 20\Gamma$ , and  $T = 0.4\Gamma$ . Circles, squares, diamonds, and triangles (solid, dashed, dotted, and dotted-dashed lines) refer to  $U = -2\Delta = 0, \Gamma, 2\Gamma$ , and  $4\Gamma$ , respectively.

#### IV. PERTURBATION THEORY IN INTERACTION

As a next step, we investigate the change of the dot transient dynamics due to the finite Coulomb repulsion, which is described by the term (4) in the Hamiltonian. In the regime where  $U$  is small compared to the other energy scales, we can employ a perturbative expansion which we truncate after the first order. Note that as the interaction involves electrons of opposite spins, we have to keep track of the spin indices henceforth.

In order to calculate the time-dependent dot population  $n_\sigma(t)$ , we start from Eq. (15) and expand the dot GF to first order in  $U$ . Discarding all disconnected diagrams, this leads to

$$D_\sigma^{(1)}(t, t') = U \int_C ds n_{\bar{\sigma}}(s) D_\sigma(t, s) D_\sigma(s, t'). \quad (41)$$

The superscript denotes the first order in  $U$ , while the GFs on the right hand side and the particle density  $n_{\bar{\sigma}}(s)$  are the respective functions for the noninteracting case. The time integration runs along the Keldysh contour  $C$ . The lesser GF can be expressed in terms of the advanced and retarded GFs and reads

$$D_\sigma^{(1)<}(t, t') = U \int_{-\infty}^{\infty} ds n_{\bar{\sigma}}(s) [D_\sigma^R(t, s) D_\sigma^<(s, t') + D_\sigma^<(t, s) D_\sigma^A(s, t')]. \quad (42)$$

Both components can be combined by using the complex conjugation properties

$$\begin{aligned} D_\sigma^A(t, t') &= [D_\sigma^R(t', t)]^*, \\ D_\sigma^<(t, t') &= -[D_\sigma^<(t', t)]^*. \end{aligned} \quad (43)$$

Initially, before the coupling to the leads is switched on, the dot is assumed to be empty, which means that  $n_{\bar{\sigma}}(s) = 0$  for  $s < 0$ . Therefore, we can rewrite the first order correction to the dot occupation number as

$$n_{\sigma}^{(1)}(t) = 2 U \text{Im}[r_{\sigma}(t)], \quad (44)$$

where

$$r_{\sigma}(t) = \int_0^t ds n_{\bar{\sigma}}(s) D_{\sigma}^R(t, s) D_{\sigma}^<(s, t) \quad (45)$$

depends only on properties of the noninteracting system and is thus accessible. In the WFB limit, this calculation can mostly be done analytically using the functions given in Eqs. (23) and (25).

In order to keep the derivation simple, we shall investigate the case  $\Delta = 0$  in equilibrium and at zero temperature ( $V = T = 0$ ). The change in the asymptotic value can most easily be accessed, because the usual perturbation theory in the frequency domain can be employed. One finds the following correction to the dot occupation,

$$n_{\sigma, \text{stat}}^{(1)} = -iU n_{\bar{\sigma}, \text{stat}}^{(0)} \int \frac{d\omega}{2\pi} D_{\sigma}^<(\omega) [D_{\sigma}(\omega) - \tilde{D}_{\sigma}(\omega)]. \quad (46)$$

Using the well-known expressions for the dot GFs  $D_{\sigma}^{ij}(\omega)$ , and the fact that the unperturbed stationary dot occupation is given by  $n_{\sigma, \text{stat}}^{(0)} = 1/2$ , one finds

$$n_{\sigma, \text{stat}}^{(1)} = -\frac{U}{2\pi\Gamma}, \quad (47)$$

which is a simple reduction of the stationary value due to the Coulomb repulsion. In a next step, we shall find out how this stationary value is approached. For this purpose, we evaluate the function (45) which contains the unperturbed time-dependent occupation number. For our choice of parameters, this function can be read off from Eq. (26):

$$n_{\bar{\sigma}}^{(0)}(t) = \frac{1}{2} (1 - e^{-2\Gamma t}). \quad (48)$$

Hence, in equilibrium the dot occupation without Coulomb interaction saturates exponentially on a time-scale  $\Gamma^{-1}$ . Moreover, we need the lesser dot GF which can be derived from Eq. (16). One finds

$$D_{\sigma}^<(s, t) = -\frac{i\Gamma}{\pi} \int_{-\infty}^0 \frac{d\omega}{\Gamma^2 + \omega^2} \times [e^{-i\omega(s-t)} - e^{-\Gamma s} e^{i\omega t} - e^{-\Gamma t} e^{-i\omega s} + e^{-\Gamma(s+t)}]. \quad (49)$$

For  $\Delta = 0$ , the retarded GF (25) becomes purely imaginary and the only imaginary part in Eq. (45) arises from the lesser GF  $D_{\sigma}^<(s, t)$ . Therefore, we only need to evaluate the imaginary part of the  $\omega$ -integrals. With the definition<sup>34</sup>

$$z(t) := \text{Im} \int_{-\infty}^0 d\omega \frac{e^{i\omega t}}{\Gamma^2 + \omega^2} \quad (50) \\ = \frac{\text{sgn}(t)}{\Gamma} [\text{Chi}(\Gamma|t) \sinh(\Gamma|t) - \text{Shi}(\Gamma|t) \cosh(\Gamma|t)],$$

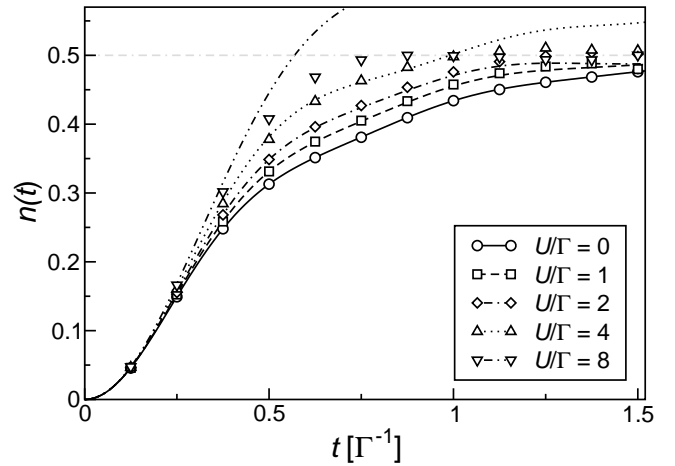


FIG. 4: Time-dependent dot occupation for different interaction strengths  $U$  ( $V = 0$ ,  $\Delta = -U/2$ ,  $\epsilon_c/\Gamma = 10$ ,  $T = 0.2\Gamma$ ). Curves show the results from the first order perturbation calculation in  $U$ . The symbols represent the MC data.

where  $\text{Shi}(x)$  and  $\text{Chi}(x)$  denote the hyperbolic sine and cosine integral functions, respectively, we obtain

$$n_{\sigma}^{(1)}(t) = \frac{2U\Gamma}{\pi} \int_0^t n_{\bar{\sigma}}^{(0)}(s) e^{-\Gamma(t-s)} \times [z(t-s) - e^{-\Gamma s} z(t) + e^{-\Gamma t} z(s)]. \quad (51)$$

This integral is evaluated numerically for arbitrary  $t$ . As the integrand is regular towards  $s, t \rightarrow 0$ , one concludes that the time derivative vanishes for small times and the correction due to the Coulomb interaction only sets in gradually. This is understandable since we assumed the dot to be initially unoccupied and the Coulomb interaction can only have an effect once a finite population has been established on the dot.

The previous calculations for  $V = \Delta = T = 0$  clearly present an oversimplified picture. Although the qualitative statements remain correct, additional energy scales due to finite temperature, asymmetry, voltage, and bandwidth render the whole picture more complicated. In these cases, however, an all-numerical scheme has to be used. We chose to solve the integral equation (13) by discretizing the time axis and thus translating it into a matrix equation.

In order to investigate the limit of the approximation in  $U$ , we compared the perturbative corrections to MC results which are exact for any interaction strength. In Fig. 4, we plot the time-dependent occupation probability for a single spin orientation in the noninteracting model and for a relatively small interaction  $U$ . While for small times, the graphs coincide within numerical accuracy, deviations become visible after a time of order  $\Gamma^{-1}$ . This is not surprising because in order for the interaction term to be fully operational a finite dot population is necessary. This process requires a time of the order  $\Gamma^{-1}$ .

In order to investigate the interaction effect more

closely, we plot in Fig. 5 the interaction correction for several values of  $U$ . One notices a good agreement up to times of order  $\Gamma^{-1}$  even for interaction strengths as large as  $U = \Gamma$ , which is actually beyond the range of the perturbation theory. In this regime, even an expansion up to second order in  $U$ , albeit feasible in principle, would not lead to a more reliable result. For this reason, we only consider the first order in  $U$ .

While the effect of the Coulomb interaction on the displacement current can be calculated by differentiating Eq. (51) with respect to time, we still have to investigate the time dependence of the average current. As we argued previously, its dependence on the electronic bandwidth is very small, so we shall do this analysis in the WFB limit. The calculation starts again from Eqs. (21) and (22), where we have to use the first order expansions of the dot GFs. Hence the expression for the current across, say, the left lead, is given by a sum of two terms  $I_L^{(1)} = I_L^{\prime(1)}(t) + I_L^{\prime\prime(1)}(t)$ , where the first one is proportional to the dot occupation

$$I_{L\sigma}^{\prime(1)}(t) = \Gamma \Theta(t) n_{\sigma}^{(1)}(t). \quad (52)$$

The derivation of the second contribution involves the complete set of dot GFs,  $D^K$ ,  $D^R$  and  $D^A$ . A straightforward calculation then leads to the following result which is valid at zero temperature,

$$I_{L\sigma}^{\prime\prime(1)}(t) = \frac{eU\Gamma}{\pi} \int_0^t ds \frac{e^{-\Gamma(t-s)}}{t-s} \times \left\{ \frac{1}{2} - \cos[|V/2 - \Delta|(t-s)] \right\} \int_s^t ds' n_{\sigma}^{(0)}(s'). \quad (53)$$

This integral can be calculated numerically using the known zero-order dot population  $n_{\sigma}^{(0)}(t)$ . The result is compared with the MC data in Fig. 6. In contrast to the dot occupation, the agreement between perturbation theory and numerically exact MC simulations for the current degrades rapidly towards stronger interaction, see Fig. 6 for  $U = 8\Gamma$ . The steady state value of the current is considerably smaller than that for weak interactions. However, this does not contradict the conventional Kondo picture, where the conductance is enhanced, since in our case the voltage is higher than the interaction strength. Another feature is the extremely weak oscillations in relation to the small  $U$  case, which can be interpreted as a precursor of the Kondo physics as discussed in [21].

## V. MONTE CARLO SIMULATIONS AT ARBITRARY INTERACTION STRENGTH

To go beyond the first order perturbation theory, we employ a numerically exact diagrammatic Monte Carlo scheme. The method is a generalization of the algorithm proposed in Ref. [35], or – equivalently – the Keldysh implementation of the diagrammatic impurity solver of Ref. [36]. Here, we only outline the basic concepts of the

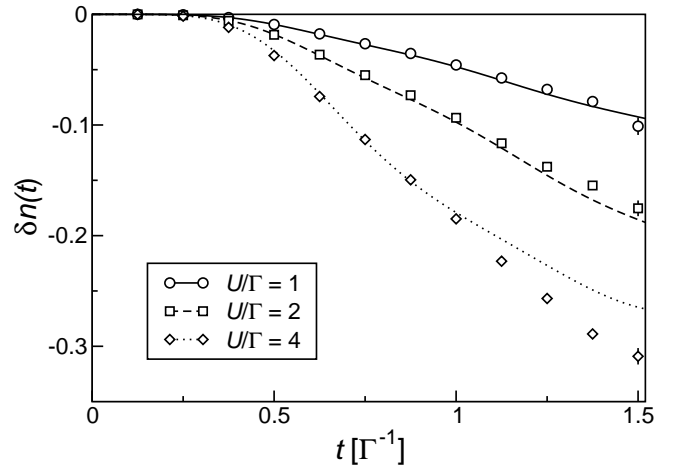


FIG. 5: Change of the time-dependent dot occupation due to interactions,  $\delta n_{\sigma}(U) = n_{\sigma}(U) - n_{\sigma}(U = 0)$ , for several values of the interaction strength.  $V = 0$ ,  $\Delta = -U/2$ ,  $\epsilon_c/\Gamma = 10$ ,  $T = 0.2\Gamma$ . Curves show the results from the first order perturbation calculation in  $U$ . The symbols represent the MC data.

algorithm and refer to Refs. [35,36] for further details; the specific aspects of dealing with the electron-electron correlations in the real-time simulations will be presented in a forthcoming publication.

The main idea is to evaluate the expectation value  $\langle O(t) \rangle = \text{Tr}_{\text{dot,lead}} [\varrho_0^{\text{dot,lead}} e^{itH} O e^{-itH}]$  by stochastically sampling a perturbation expansion in the tunneling term  $H_T$ . To this end, we employ an interaction representation in which the time evolution along the Kadanoff-Baym contour  $0 \rightarrow t \rightarrow 0$  is determined by  $H_{\text{loc}} + H_0 = H_{\text{dot}} + H_U + H_0$  and rewrite the time evolution operators  $e^{\pm itH}$  as (anti-)time ordered exponentials

$$\langle O(t) \rangle = \text{Tr}_{\text{dot,lead}} \left[ \varrho_0^{\text{dot,lead}} \tilde{T} e^{i \int_0^t ds H_T(s)} O(s) T e^{-i \int_0^t ds H_T(s)} \right], \quad (54)$$

with  $O(s) = e^{it(H_{\text{loc}}+H_0)} O e^{-it(H_{\text{loc}}+H_0)}$  (and  $H_T(s)$  accordingly). The exponentials are then expanded into a power series, which allows to trace out the electrode degrees of freedom in an exact manner. At perturbation order  $N$  (for given spin), this yields a determinant of an  $N \times N$  matrix whose elements are determined by the self-energy and the times at which the tunneling events occur. The configuration space consists of all possible sequences of dot creation and annihilation operators on the Kadanoff-Baym contour, and the MC sampling proceeds through local updates of these operator sequences (insertion/removal of pairs of creation and annihilation operators, or shifts of the operator positions). We use both a continuous-time implementation (CTQMC) as well as one which utilizes a discretization scheme for the real-time axis to speed up the sampling process (DQMC). While the continuous-time approach is completely free of systematic errors, we kept discretization effects be-

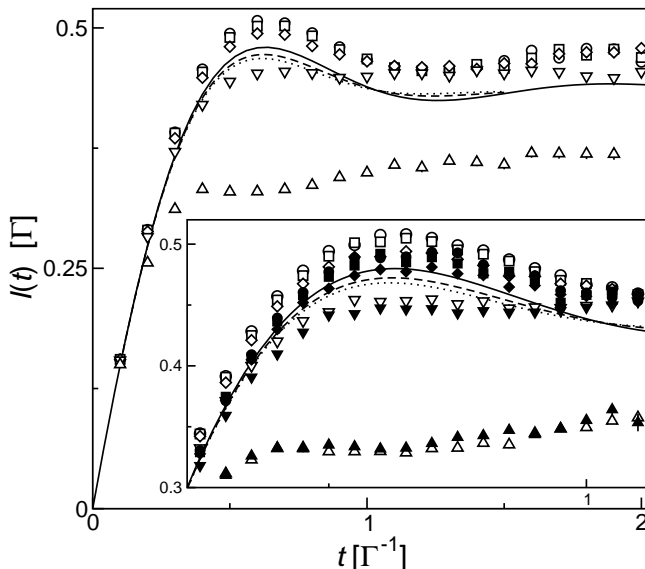


FIG. 6: DQMC data for the total current  $I(t)$  (symbols) and results according to Eqs. (52) and (53) (lines) for  $V = 10\Gamma$ ,  $T = 0$ , and  $\epsilon_c = 10\Gamma$  and  $40\Gamma$  (open and filled symbols, respectively). A WFB was assumed for the first order perturbation calculation. Circles, squares, diamonds, and triangles (facing down and up) refer to  $\Delta = -U/2$  and  $U = 0, \Gamma, 2\Gamma, 4\Gamma$ , and  $8\Gamma$ , respectively, while solid, dashed, and dotted lines refer to  $U = 0, \Gamma$ , and  $2\Gamma$ .

low statistical errors in the discrete time implementation as well, by using a fine mesh of  $10^3$  points along the real-time axis. From the simulation, we obtain the time-dependent dot population  $n(t)$  as well as  $I_{L,R}(t)$ ,  $I_{\text{disp}}(t)$ , and the total current  $I(t)$ .

While this simulation approach can handle arbitrary interaction strengths, it suffers from a dynamical sign problem<sup>42</sup> which becomes severe at long times or for large bandwidth. We find that the error bars grow exponentially with average perturbation order, and thus exponentially with time  $t$ . In the noninteracting model, which factorizes into spin-up and -down components, only one spin species needs to be simulated. This reduces the average perturbation order by a factor of two and allows us to simulate a time interval which is about twice as long as in an interacting model (in contrast to imaginary time, the perturbation order is essentially independent of interaction strength). Our simulations of the interacting AIM can reach the stationary state for certain parameters (cf. Fig. 6), but not yet for in the general case. We note in passing that in principle, the inclusion of a phonon background coupling to the interacting dot is straightforward within the path-integral framework of Ref. [35], or using the method proposed in Ref. [37].

## VI. DISCUSSION AND CONCLUSIONS

After switching on the tunneling, the dynamics of the AIM exhibits a surprisingly rich transient behavior. The reason can be found in the abundance of different energy scales. While in the steady state, all parameters like temperature  $T$ , voltage  $V$ , contact transparency  $\Gamma$ , and dot parameters – the bare energy  $\Delta$  and the interaction strength  $U$  – are known to be decisive for the stationary values of the transport current as well as the population probability of the dot, in the opposite limit of intermediate and especially short times the dynamics is dominated by the influence of  $\Gamma$  and  $\Delta$ . In fact, in both the interacting and the noninteracting case the typical timescale at which the steady state is reached is of the order  $\Gamma^{-1}$ . In the noninteracting case it is clearly visible that the approach towards steady state is exponential, see Eqs. (26) and (31). On the other hand, a nonzero detuning  $\Delta$  or a finite band cutoff lead to superimposed oscillations of the observables' time evolution.

The most interesting behavior is encountered at very short timescales. It turns out that the rather simple WFB theory fails to give meaningful results here, predicting e.g. an instantaneous finite value for the currents through the individual contacts (36). This unphysical picture can only be corrected by considering a more realistic model for the electrodes featuring a finite bandwidth  $\epsilon_c$ , which then dominates the short time dynamics of the system. It slows down the onset of the current and dot population and thus quenches their time derivative to much smaller values than for an infinite cutoff. Only after a timescale of the order of  $\epsilon_c^{-1}$  do current and dot population approach the values of the WFB model.

However, this comes as no surprise since for a system with a finite range of allowed excitations  $W$  (in our case the electrodes with  $W \sim \epsilon_c$ ), the uncertainty principle demands that the reaction to any instantaneous perturbation (switching on of tunneling) has to take place on a finite timescale  $\sim W^{-1}$ . Furthermore, the MC simulations reveal fast oscillations in the currents through the individual contacts, whose wavelength and amplitude decreases with increasing  $\epsilon_c$ .

In contrast to the currents through the electrodes and the displacement current, however, the total current through the system is only weakly affected by the bandwidth. According to the numerical results, even for bandwidths only twice as large as the voltage, the current follows the analytical results for the WFB with high accuracy. This stems from the fact that the displacement current (29) monitors the redistribution of charge across the electrodes, but it is not responsible for any net charge flow; on the other hand, the cutoff effects are almost completely due to the charge redistribution. Therefore, it appears natural to expect the total current to be only weakly affected by the explicit value of  $\epsilon_c$ . We find virtually no influence on the long-time dynamics for realistic voltage/bandwidth quotients. The maximal deviations with respect to the WFB limit is again achieved during

times  $\sim \epsilon_c^{-1}$ .

For an initially empty dot the effects of a finite Coulomb interaction become visible only after a timescale  $\Gamma^{-1}$ . This can be rationalized by observing that the same timescale is necessary to build up a dot population large enough to be affected by electronic correlations. Furthermore, we find that the quality of the approximation by lowest order perturbation expansion is remarkably good (even for intermediate  $U$ ) up to  $t\Gamma \approx 1$ , which is about a factor of three smaller than the time required to reach the steady state.

This shows that similarly to the Kondo case of Ref. [38], the full interaction effects take a time of several  $\Gamma^{-1}$  to develop. Another interaction effect is the suppression of both the dot population and the current. While the first effect is quite natural, the second one is seemingly at odds with the common wisdom that at sufficiently low temperatures, due to the Kondo effect, the transport properties of the system must approach the unitary limit of a perfectly resonant level, see e.g. Ref. [39]. Our results do not allow to see this kind of physics for two reasons: (i) the steady state is not yet fully established, (ii) the applied voltage is rather large and therefore has the potential to destroy the Kondo ef-

fect even in the steady state regime.

To conclude, we presented a theoretical treatment of transient effects in an AIM biased with a finite voltage after a sudden switching on of the tunneling. Using exact analytical solutions and perturbation theory as well as dedicated numerical schemes (MC) we identified different regimes in the time evolution of the currents and the dot's population probability and related them to the parameters of the system. Special attention has been paid to the influence of electron-electron interactions on the dot and the bandwidth of the electrodes.

### Acknowledgments

T.L.S. is financially supported by the Swiss NSF and the NCCR Nanoscience. A.K. is supported by the DFG grant No. KO-2235/2 (Germany). L.M. acknowledges computational resources from the Black Forest Grid at the university of Freiburg. P.W. was supported by NSF-DMR-0705847. The CTQMC calculations were run on the Hreidar cluster at ETH Zurich.

- 
- <sup>1</sup> P. W. Anderson, Phys. Rev. **124**, 41 (1961).  
<sup>2</sup> A. F. G. Wyatt, Phys. Rev. Lett. **13**, 401 (1964).  
<sup>3</sup> J. Appelbaum, Phys. Rev. Lett. **17**, 91 (1966).  
<sup>4</sup> P. W. Anderson, Phys. Rev. Lett. **17**, 95 (1966).  
<sup>5</sup> A. M. Tsvelik and P. B. Wiegmann, Adv. Phys. **32**, 453 (1983).  
<sup>6</sup> N. Andrei, K. Furuya, and J. H. Lowenstein, Rev. Mod. Phys. **55**, 331 (1983).  
<sup>7</sup> D. Goldhaber-Gordon, H. Shtrikman, D. Mahalu, D. Abusch-Magder, U. Meirav, and M. A. Kastner, Nature **391**, 156 (1998).  
<sup>8</sup> S. M. Cronenwett, T. H. Oosterkamp, and L. P. Kouwenhoven, Science **281**, 540 (1998).  
<sup>9</sup> J. Schmid, J. Weis, K. Eberl, and K. von Klitzing, Physica B **256-258**, 182 (1998).  
<sup>10</sup> Y. Meir, N. S. Wingreen, and P. A. Lee, Phys. Rev. Lett. **70**, 2601 (1993).  
<sup>11</sup> T. A. Costi, Phys. Rev. B **55**, 3003 (1997).  
<sup>12</sup> J. König, H. Schoeller, and G. Schön, Phys. Rev. Lett. **76**, 1715 (1996).  
<sup>13</sup> A. Rosch, J. Kroha, and P. Wölfle, Phys. Rev. Lett. **87**, 156802 (2001).  
<sup>14</sup> M. H. Hettler, J. Kroha, and S. Hershfield, Phys. Rev. B **58**, 5649 (1998).  
<sup>15</sup> A. Oguri, J. Phys. Soc. Jap. **71**, 2969 (2002).  
<sup>16</sup> A. Komnik and A. O. Gogolin, Phys. Rev. B **69**, 153102 (2004).  
<sup>17</sup> S. Weiss, J. Eckel, M. Thorwart, and R. Egger, Phys. Rev. B **77**, 195316 (2008).  
<sup>18</sup> R. M. Konik, H. Saleur, and A. Ludwig, Phys. Rev. B **66**, 125304 (2002).  
<sup>19</sup> A.-P. Jauho, N. S. Wingreen, and Y. Meir, Phys. Rev. B **50**, 5528 (1994).  
<sup>20</sup> M. Plihal, D. C. Langreth, and P. Nordlander, Phys. Rev. B **71**, 165321 (2005).  
<sup>21</sup> A. Goker, B. A. Friedman, and P. Nordlander, J. Phys.: Condens. Matter **19**, 376206 (2007).  
<sup>22</sup> J. Maciejko, J. Wang, and H. Guo, Phys. Rev. B **74**, 085324 (2006).  
<sup>23</sup> A. Komnik and A. O. Gogolin, Phys. Rev. Lett. **90**, 246403 (2003).  
<sup>24</sup> P. Mehta and N. Andrei, Phys. Rev. Lett. **96**, 216802 (2006).  
<sup>25</sup> E. Boulat and H. Saleur, Phys. Rev. B **77**, 033409 (2008).  
<sup>26</sup> C. Caroli, R. Combescot, P. Nozieres, and D. Saint-James, J. Phys. C **4**, 916 (1971).  
<sup>27</sup> E. M. Lifshits and L. P. Pitaevskii, *Physical Kinetics* (Pergamon Press, Oxford, 1981), we are using the notation of this book.  
<sup>28</sup> D. C. Langreth, in *Linear and nonlinear electron transport in solids*, edited by J. J. Devreese and V. E. van Doren (Plenum, New York, 1976), vol. 17 of *NATO ASI, Series B*.  
<sup>29</sup> G. Mahan, *Many-Particle Physics* (Plenum press, 1991).  
<sup>30</sup> D. C. Langreth and P. Nordlander, Phys. Rev. B **43**, 2541 (1991).  
<sup>31</sup> M. Büttiker, A. Prêtre, and H. Thomas, Phys. Rev. Lett. **70**, 4114 (1993).  
<sup>32</sup> J. Fransson, O. Eriksson, and I. Sandalov, Phys. Rev. B **66**, 195319 (2002).  
<sup>33</sup> M. Plihal, D. C. Langreth, and P. Nordlander, Phys. Rev. B **61**, R13341 (2000).  
<sup>34</sup> I. Gradshteyn and I. Ryzhik, *Table of Integrals, Series and Products* (Academic Press, Dover, 1975).  
<sup>35</sup> L. Mühlbacher and E. Rabani, Phys. Rev. Lett. **100**, 176403 (2008).

- <sup>36</sup> P. Werner, A. Comanac, L. de' Medici, M. Troyer, and A. J. Millis, Phys. Rev. Lett. **97**, 076405 (2006).
- <sup>37</sup> P. Werner and A. J. Millis, Phys. Rev. Lett. **99**, 146404 (2007).
- <sup>38</sup> P. Nordlander, M. Pustilnik, Y. Meir, N. S. Wingreen, and D. C. Langreth, Phys. Rev. Lett. **83**, 808 (1999).
- <sup>39</sup> A. Kaminski, Y. V. Nazarov, and L. I. Glazman, Phys. Rev. B **62**, 8154 (2000).
- <sup>40</sup> We assume the electrodes to be large enough in order to have a meaningful concept of temperature.
- <sup>41</sup> At finite temperature the single particle levels can be considered as broadened, having the typical width of  $T$ . That is why it is natural to assume the band boundaries to be widened with  $\eta \approx T$ .
- <sup>42</sup> In imaginary time, the diagrammatic Monte Carlo simulation of the AIM does not encounter a sign problem. All the (fermionic) sign cancelations between crossing and non-crossing diagrams can be absorbed into the determinant of self-energies (hybridization functions), and the imaginary time evolution  $e^{-H_{loc}\tau}$  gives a real contribution to the weight. In real-time diagrammatic Monte Carlo, both the self-energies and the time evolution operator are complex.